JOURNAL OF PETROLOGY | VOLUME 46 | NUMBER 4 | PAGES 783–798 | 2005 | doi:10.1093/petrology/egh097

An Experimental Study of the Sulfur Content in Basaltic Melts Saturated with Immiscible Sulfide or Sulfate Liquids at 1300°C and 1·0 GPa

PEDRO J. JUGO*, ROBERT W. LUTH AND JEREMY P. RICHARDS

DEPARTMENT OF EARTH & ATMOSPHERIC SCIENCES, UNIVERSITY OF ALBERTA, EDMONTON, ALBERTA, CANADA, T6G 2E3

RECEIVED JANUARY 10, 2004; ACCEPTED NOVEMBER 18, 2004
ADVANCE ACCESS PUBLICATION JANUARY 7, 2005

The sulfur content in basaltic melts coexisting with either sulfide or sulfate melts was determined experimentally. The experimental conditions were in the range of 1300–1355°C and 1·0–1·6 GPa, conditions appropriate for the melting of the upper mantle above subduction zones. Under these conditions, both sulfide and sulfate were present as immiscible liquids, as inferred from the round geometries of the quenched sulfide and sulfate phases. The measured S content in basaltic melts saturated with sulfate liquids ([S] = 1·5 ± 0·2 wt %) was 10 times higher than the S content in basaltic melts saturated with sulfide liquids ([S] = 0·14 ± 0·02 wt %). In our experiments, sulfate liquids were stable at fO_2 as low as $\Delta FMQ = +1{\cdot}85$ [$\Delta FMQ = \log (fO_2)_{sample} - \log (fO_2)_{FMQ}$, where FMQ is the fayalite–magnetite–quartz oxygen buffer], and evidence from other sources indicates that sulfates will be stable at lower fO_2 in melts with lower activities of silica. Because chalcophile and highly siderophile elements, such as Cu, Ni, Au, and Pd, are partitioned preferentially into sulfide phases, melting of sufficiently oxidized sources, in which sulfides are not stable, would favor incorporation of these elements into the silicate melt produced. Such melts would have a higher potential to generate ore deposits. This study shows that the high sulfur contents of such oxidized basalts also means that relatively small amounts of such magmas can provide significant amounts of sulfur to exsolving volatile phases and account for the bulk of the sulfur expelled in some volcanic eruptions, such the 1991 eruption of Mount Pinatubo.

KEY WORDS: *basalt; mantle; oxidation state; sulfate; sulfur*

INTRODUCTION

Although sulfur is a minor element in the Earth (250 ± 50 ppm, the 11th most abundant element in the Silicate Earth; McDonough & Sun, 1995), it has a disproportionate impact on the geochemical behavior of some elements because S commonly occurs as discrete sulfide phases. Thus, sulfides largely control the behavior of chalcophile (e.g. Cu, Ni) and highly siderophile elements (Ru, Rh, Pd, Re, Os, Ir, Pt, and Au), elements that are of interest because they provide valuable information about geochemical processes and because they are economically important. For these reasons, the solubility of S as sulfide and the stability of sulfide minerals in silicate melts have been widely investigated experimentally as functions of pressure, temperature, and melt composition (e.g. see Poulson & Ohmoto, 1990, for a compilation of experimental work until 1990; Mavrogenes & O'Neill, 1999; Holzheid & Grove, 2002; O'Neill & Mavrogenes, 2002). Consequently, these data have been used to model sulfide elimination in magmatic sources and sulfide precipitation in crystallizing melts.

Although occurrences of sulfate-bearing minerals in igneous rocks (e.g. nosean, haüyne, silvialite) were documented early in the 20th century (e.g. Lindgren & Ransome, 1906; Brauns, 1914), the assumption that S is present only as sulfide in magmatic systems was challenged only by the discovery of anhydrite in pumices erupted by El Chichón (Chiapas, Mexico) in 1982 (Luhr *et al.*, 1984). Luhr & Varekamp (1984) compared the

*Corresponding author. Present address: Institut für Mineralogie, J. W. Goethe Universität, D-60054, Frankfurt am Main, Germany. Telephone: ++49 69 798 23145. Fax: ++49 69 798 22101. E-mail: Pedro.Jugo@em.uni-frankfurt.de

© The Author 2005. Published by Oxford University Press. All rights reserved. For Permissions, please email: journals.permissions@oupjournals.org

anhydrite-bearing eruptions of El Chichón in early 1982 to the eruption of carbonatite lavas from Oldoinyo Lengai in 1960 that established the existence of carbonatitic melts. They recognized the implications of igneous anhydrite occurrences and concluded that the El Chichón eruptions 'seem destined to alter many of our concepts regarding the role of S in magmatism and the relationship between explosive volcanism and the earth's climate' (Luhr & Varekamp, 1984, p. vii).

Subsequent experimental studies (Carroll & Rutherford, 1985, 1987; Luhr, 1990) showed that sulfates (e.g. anhydrite), not sulfides, are the stable S-bearing magmatic phases at oxygen fugacities (fO_2) above those defined by the nickel–nickel oxide (bunsenite) oxygen buffer (NNO). [ΔFMQ is used in this paper to indicate relative oxygen fugacity, where $\Delta FMQ = \log (fO_2)_{sample} - \log (fO_2)_{FMQ}$, and FMQ refers to the fayalite–magnetite–quartz oxygen buffer; for comparison purposes $\Delta NNO \approx \Delta FMQ - 0{\cdot}7$, although the exact relationship is a function of P and T.] Estimates of the oxidation state of island-arc basalts (IAB) show that they are typically more oxidized than basalts from other tectonic settings (Ballhaus, 1993; Parkinson & Arculus, 1999) and estimates of the speciation of S in some basaltic systems show a dominance of sulfate over sulfide (Nilsson & Peach, 1993; Metrich & Clocchiatti, 1996; Gurenko & Schminke, 1998, 2000; Matthews *et al.*, 1999). Therefore, solubility data for S as sulfate are needed to provide appropriate models for the behavior of S, and of chalcophile and highly siderophile elements in these environments.

Eruption products from the 1991 eruption of Mt. Pinatubo (Philippines) showed once more that anhydrite was a stable igneous phase. This eruption released more than 17 Mt of SO_2 into the atmosphere (Gerlach *et al.*, 1996) and demonstrated the significant short-term impact that high-S explosive volcanism can have on global climate (e.g. cooling of the order of 0·5°C over large parts of the Earth and significant increase of the ozone depletion rates; Self *et al.*, 1996). At Mt. Pinatubo, intrusion of basaltic magmas into a large gas-charged dacitic body followed by explosive eruption is well documented for the 1991 eruption and for prehistoric eruptions (Newhall *et al.*, 1996; Pallister *et al.*, 1996). De Hoog *et al.* (2003) estimated that the oxidation state of the basaltic melt involved in this eruption was similar to that of the dacitic magma ($\Delta FMQ = +2{\cdot}1$), showing that mixing between the dacitic and the basaltic magma did not result in significant changes in fO_2 as suggested in some models for the 1991 Pinatubo eruption (e.g. Hattori, 1993; Kress, 1997).

Estimates of the stratospheric loading of H_2SO_4 following the eruption of the Huaynaputina, Peru, in 1600 are consistent with this eruption causing the low temperatures for the summer of 1601, which were among the coldest in 1500 years in Fennoscandia (de Silva & Zielinski, 1998). A similar temporal link has been established between the low temperatures recorded in 1816 ('the year without summer') and the eruption of Tambora (Sumbawa island, Indonesia) in April 1815. This eruption produced an estimated stratospheric loading of $\sim$200 Mt H_2SO_4 and is considered the greatest S-producing eruption of the last 750 years (Stothers, 1984; de Silva & Zielinski, 1998; Palmer *et al.*, 2001). If high-S volcanic eruptions are associated with, and perhaps triggered by, oxidized basaltic melts (as in Mt. Pinatubo), modeling of these processes needs to account for S being present as sulfate in the basalts.

In this paper we present the first experimental data on the S content in basaltic melts saturated with sulfate phases, and show that partial melting of oxidized mantle sources will produce magmas enriched in sulfur and chalcophile and siderophile elements relative to those produced from sulfide-saturated sources. Such magmas may have elevated potential for forming ore deposits of these elements, and may contribute to the S budget in explosive volcanism.

EXPERIMENTAL AND ANALYTICAL METHODS

Starting materials

Three sets of experiments were performed in this study: (1) sulfide-saturated runs, produced from sulfide-bearing starting materials; (2) sulfate-saturated runs, produced from sulfate-bearing starting materials; (3) sulfide-saturated runs, produced by reduction from sulfate-bearing starting materials ('sulfate-reduction runs'). Each set of experiments required the combination of different starting materials; however, bulk compositions and experimental conditions were kept as similar as possible to isolate the effect of oxidation state on the behavior of S.

Starting materials that would yield a basaltic melt coexisting with a lherzolitic residue were used to simulate conditions of partial melting under pressures and temperatures appropriate for the upper mantle. Because these experiments were also used to study the behavior of Pd, Ir, Pt, and Au, small amounts of these metals were also added. The results pertaining to the behavior of these metals will be presented elsewhere.

Glasses

Three synthetic glasses (compositions listed in Table 1) were prepared as starting material. Suitable chemical compositions were selected among various melt compositions from previous experimental work on partial melting of peridotitic mantle (e.g. Jaques & Green, 1980; Gaetani & Grove, 1998; Robinson *et al.*, 1998). We used chemical

Table 1: Composition of glasses and olivine (KR-37) used as starting materials

	Glasses			Olivine	Gaetani & Grove (1998)			This work	
				KR-37					
	B302	Low-Ca	Low-Fe		Basalt 82-72f	Peridotite FP1	70:30 bas:per	Ca-mix 10·76:1	Fe-mix 9·54:1
SiO_2	46·9 (4)	48·9 (3)	49·2 (3)	40·4 (2)	47·70	44·90	46·87	46·97	46·83
TiO_2	0·67 (4)	0·49 (3)	0·50 (4)		0·62	0·18	0·49	0·47	0·48
Al_2O_3	17·6 (1)	15·3 (1)	15·6 (1)		19·05	4·27	14·63	14·69	14·85
Cr_2O_3	0·10 (2)	0·15 (2)	0·24 (3)		0·12	0·57	0·25	0·14	0·23
FeO	9·0 (1)	8·2 (1)	3·37 (6)	9·1 (2)	7·82	7·58	7·75	7·88	7·93
MgO	12·8 (2)	19·7 (3)	19·8 (3)	50·0 (3)	10·49	38·04	18·74	18·92	18·84
CaO	10·8 (1)	5·95 (7)	9·7 (1)	0·04 (2)	11·75	4·28	9·51	9·39	9·23
Na_2O	2·1 (2)	1·6 (1)	1·7 (3)		2·35	0·38	1·76	1·54	1·62
Total	99·9	100·3	100·2	99·5	99·9	100·2	100	100*	100*
Mg-no.				0·907					
n	87	30	27	15					

Numbers in parenthesis are the 1σ uncertainties associated with the last significant figure. Ca-mix, mixture of low-Ca glass and $CaSO_4$. Fe-mix, mixture of low-Fe glass and $FeSO_4$. *n*, number of analyses.
*Normalized S-free.

compositions of starting materials and run products from the experimental work of Gaetani & Grove (1998), simplified by eliminating Mn, K, and P, which are minor or trace elements that are unlikely to affect the phase equilibria studied here. One glass (labeled B302) was prepared to match the composition of the basaltic glass produced in run B302 of Gaetani & Grove (1998), because it coexisted with a spinel lherzolite assemblage at *P–T* conditions similar to those of this study. Two other glasses ('low-Ca glass' and 'low-Fe glass') were prepared to produce similar bulk compositions after specific amounts of $CaSO_4$ or $FeSO_4$ were added (calculated S-free in Table 1). Thus, the bulk compositions of 10·76:1 mixtures (by weight) of 'low-Ca glass' + $CaSO_4$ are similar to 9·54:1 mixtures of 'low-Fe glass' + $FeSO_4$. Both glass–sulfate mixtures are roughly equal in bulk composition to a combination of the 70:30 basalt–peridotite (by weight) mixture used as starting material by Gaetani & Grove (1998) plus 5 wt % SO_3 (Table 1).

All glasses were prepared from high-purity oxides and carbonates, which were ground and mixed thoroughly in an agate mortar under ethanol, partially decarbonated at 350°C for 4 h, fused in a Pt crucible at 1400°C for 30 min, and quenched by dipping the crucible in water. Pieces of the quenched glasses were inspected with a petrographic microscope at 200× for the presence of crystals. Partially crystalline glasses (containing small pieces of spinel) were ground again and fused at higher temperatures (in 25°C increments, up to 1450°C) until the quenched glasses were optically homogeneous and free of crystals, then ground and fused once more at the established melting temperatures. Random pieces of the resulting glass were mounted for electron microprobe analysis (EMPA) to test for chemical composition and homogeneity. The remaining glass was ground and stored in glass vials in a desiccator.

Sulfur

Sulfur was added as FeS, $CaSO_4$, or $FeSO_4{\cdot}H_2O$ (ferrosulfate monohydrate). The ferrosulfate monohydrate was prepared by dehydrating ferrosulfate heptahydrate ($FeSO_4{\cdot}7H_2O$) at 120°C. Amounts of ferrosulfate monohydrate equivalent to the desired amount of anhydrous ferrosulfate ($FeSO_4$) were loaded into the capsules, which were heated at 350°C for 30–60 min immediately before welding to remove the remaining H_2O.

Other phases

To promote crystallization of olivine, some runs were seeded with small amounts of finely crushed (<325 mesh), handpicked olivine crystals (KR-37, Fo_{91}; composition shown in Table 1) from West Kettle River, British Columbia (Fujii & Scarfe, 1982; Canil *et al.*, 1990). Some of the 'sulfate-reduction' experiments used small amounts of graphite powder as a reducing agent when run in Au–Pd capsules, and in a few experiments small amounts of Cr_2O_3 powder were mixed with the other starting materials to promote nucleation and growth of spinel crystals.

Table 2: Composition of the experiments in terms of phases added and resulting bulk composition

	Sulfate-saturated runs									Sulfate reduction				
Run no.:	26	30A	30B	34	35A	50	52A	56A	56B	27	35B	52B	54A	54B
Capsule type:	AuPd	AuPd	AuPd	AuPd	AuPd	AuPd	AuPd	AuPd	AuPd	C–Pt	C–Pt	C–Pt	AuPd	AuPd
Glass														
low-Ca glass		44·80		30·66	30·91			34·75		6·70	14·07		35·00	
low-Fe glass			41·26						33·90					33·08
B302 glass	49·23			8·39		50·33	49·14	36·13	35·96			16·40	38·45	37·09
Sulfate														
$CaSO_4$	5·29	4·17		2·83	2·91	5·03		3·20		0·58	1·32		3·38	
$FeSO_4{\cdot}H_2O$			5·23				4·95		4·23			1·65		3·89
Other phases														
Olivine KR-37	2·94					5·04	4·92	1·81	1·81			1·64	1·99	1·85
Graphite				0·49									0·84	0·77
Cr_2O_3								0·11	0·11				0·44	0·39
SiO_2	42·3	44·6	44·1	45·1	44·6	42·5	42·8	45·6	45·4	44·9	44·6	42·8	45·3	45·3
TiO_2	0·57	0·45	0·45	0·49	0·45	0·56	0·56	0·54	0·54	0·45	0·45	0·56	0·54	0·55
Al_2O_3	15·1	13·9	14·0	14·7	13·9	14·7	14·8	15·3	15·4	14·0	13·9	14·8	15·3	15·4
Cr_2O_3	0·09	0·14	0·22	0·13	0·14	0·08	0·08	0·26	0·29	0·14	0·14	0·08	0·67	0·67
FeO	8·2	7·5	7·8	7·8	7·5	8·3	11·9	8·2	8·4	7·5	7·5	11·9	8·2	8·3
MgO	13·5	18·0	17·8	16·9	18·0	14·9	15·0	16·3	16·2	18·1	18·0	15·0	16·1	16·1
CaO	13·1	8·9	8·7	9·3	9·0	12·4	9·1	9·6	9·5	8·7	9·0	9·1	9·6	9·5
Na_2O	1·80	1·46	1·53	1·59	1·46	1·75	1·76	1·73	1·76	1·47	1·46	1·76	1·72	1·77
SO_3	5·41	5·01	5·37	3·97	5·06	4·90	3·99	2·48	2·64	4·69	5·04	3·99	2·51	2·42

AuPd, $Au_{75}Pd_{25}$ or $Au_{80}Pd_{20}$ capsules; C–Pt, graphite-lined platinum capsules. Upper half of table shows masses added in milligrams; bottom half of table shows oxide composition normalized to 100%.

Bulk compositions

The first set of experiments (sulfide-saturated) used 5:1 mixtures (by weight) of B302 glass:FeS, with total masses ranging from 40·50 to 63·60 mg. The other two sets of experiments used various combinations of starting materials. Table 2 shows the type and amount of starting material added in these experiments (except precious metals) as well as the bulk composition of each run in terms of oxides.

Capsule materials

Graphite-lined platinum capsules were used for most of the sulfide-saturated experiments because the presence of graphite holds the oxidation state in this type of experiment at reducing conditions (Ulmer & Luth, 1991; Holloway *et al.*, 1992). The reducing effect of graphite prohibited its use in sulfate-saturated experiments, making the choice of capsule material the major limitation for these experiments. Unlined Pt capsules are unusable because Pt reacts with both Fe and S in the charge, resulting in Fe loss by formation of Fe–Pt alloy, and capsule corrosion by formation of PtS. Gold is effectively inert under these conditions but its relatively low melting point (1064°C at 1 atm) makes it unsuitable for the temperatures of this study (1300°C). Capsules made of Au–Pd alloys ($Au_{75}Pd_{25}$ and $Au_{80}Pd_{20}$, by weight) have sufficiently high melting points (>1350°C at 1 atm; Massalski, 1986). These alloys reacted slowly with S to form PdS, which weakened the alloy and limited the duration of experiments to approximately 6 h. We determined, however, that sulfate-saturated experiments reached equilibrium after only 2 h. Therefore, we used this capsule material in some of the sulfate-reduction experiments and all the sulfate-saturated experiments. Au–Pd capsules were used only at temperatures below 1325°C to provide a safety margin in temperature between the run conditions and the melting point of the alloy.

Experimental methods

For all the experiments, an end-loaded, solid-media, piston-cylinder apparatus (Boyd & England, 1960;

Dunn, 1993) was used. The experiments used 19 mm diameter talc–Pyrex sample assemblies of the Kushiro (1976) type. The sample volume in these assemblies can accommodate one 5 mm outer diameter (o.d.) capsule up to 16 mm in length, and is large enough to accommodate two 3 mm o.d. capsules side by side, or two 5 mm o.d. capsules (and up to 8 mm length) on top of each other. Because of the constraints imposed by the Au–Pd capsules on the duration of the experiments, several paired experiments were run to test for equilibrium. Excess space in the sample volume (after loading the capsules) was filled in most experiments with crushed alumina powder. The use of crushed alumina as filler worked well in experiments using Pt capsules but Au–Pd capsules are more brittle, and broke easily when removed from the assembly at the end of the runs. Crushed Pyrex was tried as filler, but was rejected because Au–Pd capsules cracked upon quenching and molten Pyrex entered and mixed with the run products. The best results were obtained using sintered hematite as filler. The use of hematite as filler reduced significantly the cracking and fracturing of the Au–Pd capsules on quenching, probably because it did not attach as much as alumina to the capsules.

A Bourdon-tube Heise gauge with p.s.i. graduations (0–10 000 p.s.i., ~0–68·9 MPa), with 10 p.s.i. (0·0689 MPa) graduations, was used to monitor line pressure. Run pressures were kept within ±0·14 MPa of the desired pressure in all experiments. No friction correction was applied to the nominal pressure because pressure calibration of the assemblies, based on the grossular + quartz = anorthite + 2 wollastonite equilibria (Windom & Boettcher, 1976), showed that the friction correction is a function of temperature and is negligible above 1275°C.

Type-C thermocouples constructed from batch-calibrated W_5Re_{95} and $W_{26}Re_{74}$ wires (Omega Corp.) were used to measure run temperatures. At 1300°C, temperature uncertainties associated with variations in current are ~1°C. Larger uncertainties are produced by thermal gradients along the capsule volume, which are ~10°C for tapered graphite furnaces like those used in these experiments (Kushiro, 1976). The standard limits of error for type-C thermocouples at 1573 K (1300°C) are about 14°C (Dunn, 1993). Thus, the added uncertainties in temperature are about 25°C (2%). No correction was attempted for the effects of pressure or pressure gradients on the electromotive force of the thermocouples.

Analytical techniques

Elemental concentrations in all phases were determined by EMPA using wavelength-dispersive spectrometry (WDS) on a JEOL JXA-8900 electron microprobe. Typical operating conditions were 15 kV accelerating voltage and 15 nA probe current. Natural glasses and minerals (Jarosewich *et al.*, 1980) were used as standards. Matrix effects were corrected using the ZAF method. Both barite and sphalerite were used as standards for S analyses. No significant difference was detected in the use of sphalerite or barite as standards for S concentrations in the sulfide-saturated glasses, but only barite was used as a standard for sulfate-bearing runs. Glasses were mostly analyzed with beams of 10 μm diameter, although 5 μm diameter beams were used in a few runs that contained only small melt pockets. Spinel occurred as very small crystals, with cross-sections rarely larger than 3 μm, making them difficult to analyze. They were analyzed with a focused beam (~1 μm diameter) and with the inclusion of Si in the measurements as a monitor for the presence of silicates within the activation volume. Spinel crystals larger than 3 μm diameter contained <1 wt % SiO_2; hence, only analyses with <1 wt % SiO_2 were considered to be acceptable for spinel.

Control and estimation of oxidation state

Oxidation state in the experiments was constrained using combinations of starting and capsule materials. Control of oxidation state using external oxygen buffers was not possible because external buffers require the presence of a hydrous fluid phase in the charge, and water-saturated experiments in this system quench to a felt-like mixture of amphibole crystals, which means that melt compositions cannot be inferred. To impose reducing conditions, graphite-lined capsules (or small amounts of powdered graphite added to the starting materials) were used in combination with sulfide- and sulfate-bearing starting materials to produce sulfide-saturated assemblages. Conversely, oxidized starting materials (containing glasses fused in air, and sulfates) were enclosed in Au–Pd capsules to produce sulfate-saturated assemblages. Because the experiments were anhydrous and hematite was used as filler, little hydrogen diffused into the capsule from the assembly, and the oxidation state of the charges was dictated by the combination of starting materials used. Using this approach, we were able to produce runs equilibrated at fO_2 above the nickel–bunsenite buffer (NNO, ~ΔFMQ + 0·7) and below the manganosite–hausmannite buffer (MNH, ~ΔFMQ + 4). However, we could not predetermine the oxidation state of the runs, nor obtain sulfate-saturated runs equilibrated below ΔFMQ = +1·85.

The oxidation state of the experiments was estimated using the calibration of Ballhaus *et al.* (1990, 1991) for the olivine–orthopyroxene–spinel (ol–opx–spl) oxybarometer. This empirical calibration was used because Ballhaus *et al.* (1990) showed that it is more accurate

over a wider range of oxidation states than other available calibrations, and also because it does not require the chemical composition of the orthopyroxene as an input parameter [Ballhaus *et al.* (1991) estimated that the correction required for orthopyroxene-undersaturated ultramafic rocks would rarely exceed 0·2 $\log fO_2$ units]. Olivine and spinel compositions were determined by EMPA, and the Fe^{3+} content of spinel was calculated assuming stoichiometry. Although estimations of oxidation states from EMPA of spinel have been regarded as inaccurate because of the errors associated with estimation of ferric iron (e.g. Wood & Virgo, 1989; Canil *et al.*, 1990), Ballhaus *et al.* (1991) showed that the uncertainties in Fe^{3+} decrease with increasing fO_2 because of the increase in the magnetite component in spinel. Parkinson & Arculus (1999) showed that errors in fO_2 attributable to Fe^{3+} in spinel calculated from stoichiometry are significant (larger than $\sim$0·5 log units) for $Fe^{3+}/\Sigma Fe \leq 0{\cdot}2$ (corresponding to oxidation states $<\Delta FMQ = -1$), whereas for $Fe^{3+}/\Sigma Fe \geq 0{\cdot}2$, the uncertainties associated with the stoichiometric estimation of Fe^{3+} become smaller, and are insignificant (<0·2 log units) above $Fe^{3+}/\Sigma Fe \geq 0{\cdot}4$ (approximately $\Delta FMQ = +1$).

To provide an independent check on the accuracy of EMPA of spinel for the estimations of oxidation state, we routinely analyzed two spinel samples (KR-35 and KR-37) for which $Fe^{3+}/\Sigma Fe$ had previously been measured by Mössbauer spectroscopy (Canil *et al.*, 1990). The calculated fO_2 values from EMPA of both olivine and spinel using the oxybarometer calibration of Ballhaus *et al.* (1990, 1991) are $\Delta FMQ = -0{\cdot}35 \pm 0{\cdot}26$ for KR-35 (from measurements compiled during four EMPA sessions) and $\Delta FMQ = -1{\cdot}07 \pm 0{\cdot}25$ for KR-37 (from five sessions). The same calculations using the Mössbauer data for these two spinel samples (Canil *et al.*, 1990) yield $\Delta FMQ = -0{\cdot}31$ for KR-35 and $\Delta FMQ = -0{\cdot}86$ for KR-37. Our results agree within error of these values, and thus justify the use of EMPA data for the calculations of both the Fe^{3+} content in spinel and the oxidation state of our experiments. The small discrepancies between our results and those documented by Canil *et al.* (1990) are more dependent on the choice of calibration of the oxybarometer (e.g. O'Neill & Wall, 1987; Mattioli & Wood, 1988; Ballhaus *et al.*, 1990) than on the uncertainties associated with spinel analyses.

Estimation of equilibrium

Time invariance of the concentration of S in the quenched glasses was used as the criterion for equilibrium in sulfide-saturated experiments using graphite-lined Pt capsules. Experiments with duration ranging between 1 and 48 h had identical S concentrations, indicating that equilibrium was attained quickly ($t \leq 1$ h). Time invariance could not be used as a test for equilibrium in oxidized experiments because of the limitations imposed by the reaction of S with Pd in Au–Pd capsules as mentioned above. Equilibrium in these experiments was monitored by comparing run products obtained from mixtures of 'low-Ca glass' + $CaSO_4$ with run products obtained from mixtures of 'low-Fe glass' + $FeSO_4$ as starting materials. Agreement in the composition of the quenched glasses and their S content is consistent with equilibrium being achieved in these runs.

RESULTS

The results of 22 successful experiments are included in this paper. Eight sulfide-saturated runs allow comparison with available data on the S content in sulfide-saturated basaltic melts (e.g. Haughton *et al.*, 1974; Poulson & Ohmoto, 1990). Nine sulfate-saturated runs provide the first experimental data on the S content in sulfate-saturated basaltic melts. Five sulfide-saturated ('sulfate-reduction') runs complement the other experiments and helped verify equilibration of the runs. Table 3 summarizes the run conditions and the products obtained in each experiment.

Phase compositions in run products

Glasses

The glasses generated in these experiments were picrobasaltic to basaltic in composition (Table 4). All of the glasses were very similar in composition, although glasses from oxidized experiments were slightly, but consistently, more mafic ($MgO = 13{\cdot}7 \pm 1{\cdot}4$, $n = 9$) than those from sulfide-saturated runs ($MgO = 11{\cdot}8 \pm 0{\cdot}6$, $n = 13$). The S concentration in sulfate-saturated glasses ($S = 1{\cdot}5 \pm 0{\cdot}2$ wt %, $n = 9$) was $\sim$10 times higher than in sulfide-saturated glasses ($S = 0{\cdot}14 \pm 0{\cdot}02$ wt %, $n = 13$).

Sulfides

Sulfide phases had rounded shapes in polished section, which is consistent with their presence as immiscible liquids at the run conditions. They were pyrrhotitic in composition with $S = 36{\cdot}9 \pm 0{\cdot}9$ wt %, and $Fe = 60{\cdot}2 \pm 1{\cdot}2$ wt % ($n = 12$).

Sulfates

Sulfates also quenched to rounded blebs (Fig. 1), which is regarded as evidence that sulfate was present as an immiscible liquid in the oxidized runs. Polishing of sulfate-saturated samples using water to remove abrading material between polishing steps resulted in intense dissolution of the sulfates. Sulfate blebs were best preserved if samples were polished using only oil and cleaned with methanol. However, even in these cases, irregular,

Table 3: Summary of run conditions and run products

Run no.	Products	*P* (GPa)	*T* (°C)	*t* (h)
Sulfide saturated				
2	gl, sulfide, opx, cpx	1·6	1355	24
3	gl, sulfide, opx, cpx	1·6	1355	24
4	gl, sulfide, spl, opx, cpx	1·6	1355	24
5	gl, sulfide, opx, cpx	1·6	1355	24
7	gl, sulfide, spl, opx, cpx	1·6	1355	48
10	gl, sulfide	1·6	1355	1
11	gl, sulfide, opx	1·6	1355	8
12	gl, sulfide, opx, cpx	1·6	1355	4
Sulfate saturated				
26	gl, sulfate, ol, spl, opx, cpx	1·1	1315	4
30A*	gl, sulfate, spl, opx, cpx	1·2	1315	6
30B	gl, sulfate, ol, spl, opx, cpx	1·2	1315	6
34	gl, sulfate, ol, spl, opx, cpx	1·2	1315	4
35A	gl, sulfate, ol, spl, opx	1·2	1315	2
50	gl, sulfate, ol, spl	1·0	1325	4
52A	gl, sulfate, ol, spl	1·0	1300	4
56A	gl, sulfate, ol, spl	1·0	1300	4
56B	gl, sulfate, ol, spl	1·0	1300	4
Sulfate reduction				
27	gl, sulfide, ol, spl, opx, cpx	1·1	1315	10
35B	gl, sulfide, ol, spl, opx, cpx	1·2	1315	2
52B	gl, sulfide, ol, spl	1·0	1300	4
54A	gl, sulfide, ol, spl	1·0	1300	4
54B	gl, sulfide, ol, spl	1·0	1300	4

gl, glass; cpx, clinopyroxene; opx, orthopyroxene; ol, olivine; spl, spinel.
*Experiments run as pairs share the same number (e.g. 30A and 30B).

uneven, and plucked surfaces resulted because of the low hardness of the sulfates relative to the surrounding glass. For this reason, quantitative analysis of the sulfates using WDS was not possible. The wavelength of the S Kα radiation (Carroll & Rutherford, 1988) for the blebs agreed with the wavelength of the S Kα for the barite standard, confirming that the blebs were sulfates. Qualitative energy dispersive analyses (EDS) showed that the sulfates were invariably Ca- and S-rich with small amounts of Na and Mg, even in experiments in which S was added as $FeSO_4$. This latter point is taken as further supporting evidence of equilibrium between the sulfates and the melt.

Olivine

Olivine typically formed relatively large (up to 100 μm length), euhedral to subhedral crystals. Individual crystals were compositionally homogeneous, with Fo content ranging from 0·90 to 0·95 (Table 5). To verify that olivine equilibrated with the melt, the partitioning of magnesium and ferrous iron between olivine and melt (K_D, Roeder & Emslie, 1970) was calculated. Ferrous iron content in the glasses was first calculated by subtracting the ferric iron content [estimated using the method of Kilinc *et al.* (1983)] from the total iron measured as FeO by EMPA. The average K_D was $0{\cdot}32 \pm 0{\cdot}4$ for reduced experiments, and $0{\cdot}31 \pm 0{\cdot}01$ for oxidized runs (for which $0{\cdot}26 \leq Fe^{3+}/\Sigma Fe \leq 0{\cdot}49$). These values are consistent with the expected K_D ($K_D \approx 0{\cdot}33$ at 1 GPa; Ulmer, 1989) and show that olivine was in equilibrium with the silicate melt.

Spinel

Spinel was present as very small (from <1 μm and rarely up to 5 μm) equant crystals with trapezoidal sections, which were included in olivine or isolated within quenched glasses. Their compositions are shown in Table 6.

Pyroxenes

Orthopyroxene and clinopyroxene were present in some experiments (Table 3). Both pyroxenes ranged in size from a few micrometers to 15 μm diameter. Orthopyroxene crystals were usually equant, whereas the habit of clinopyroxene ranged from equant to slightly prismatic. Clinopyroxene with cores of orthopyroxene was observed in some cases. Although the compositions of these phases are not considered further in this paper, Tables 7 and 8 list compositions of clinopyroxene and orthopyroxene analyzed from the experiments.

S concentration as a function of oxidation state

Figure 2 shows measured S concentrations plotted against estimated oxidation states in the experiments. Olivine was absent in the run products from the first set of sulfide-saturated experiments, which meant that the oxidation state could not be estimated using olivine–orthopyroxene–spinel equilibria. However, because these experiments used graphite-lined capsules, their fO_2 was constrained to lie below the C–CO buffer ($\sim\Delta FMQ < -1$ at the P and T of the experiments). The rectangular box in Fig. 2 corresponds to the range in S concentration (width is $\pm 1\sigma$ standard deviation) and the approximate fO_2 range of these runs.

The lowest fO_2 in sulfate-saturated experiments was measured in run 34 ($\Delta FMQ = +1{\cdot}85$), which contained a small amount of graphite in the starting material but not enough to cause complete reduction of sulfate and saturation in sulfide (as in runs 54A and 54B). The highest fO_2 in sulfide-saturated experiments was measured in run 27 ($\Delta FMQ = -1{\cdot}12$). A drastic change in the S content occurs between the fO_2 conditions of these two

Table 4: Composition of quenched glasses (in wt %)

Run no.:	SiO_2	TiO_2	Al_2O_3	Cr_2O_3	FeO	MgO	CaO	Na_2O	S	Total*
2	47·4 (2)	0·73 (5)	18·1 (1)	0·03 (1)	8·6 (1)	11·2 (1)	11·0 (1)	2·4 (1)	0·14 (2)	99·8
3	47·9 (3)	0·68 (5)	18·2 (1)	0·05 (2)	7·0 (1)	12·1 (1)	11·4 (1)	2·3 (1)	0·13 (2)	100·0
4	47·7 (2)	0·72 (3)	18·2 (1)	0·04 (2)	8·2 (1)	11·4 (2)	11·1 (1)	2·4 (1)	0·14 (2)	100·1
5	47·9 (3)	0·74 (4)	18·3 (1)	0·05 (1)	7·9 (1)	11·5 (1)	11·4 (1)	2·4 (1)	0·14 (1)	100·5
7	47·5 (4)	0·72 (4)	18·0 (1)	0·04 (2)	8·3 (1)	11·5 (1)	10·9 (1)	2·4 (1)	0·15 (1)	99·7
10	47·1 (3)	0·68 (2)	17·8 (1)	0·08 (3)	8·2 (1)	12·6 (1)	10·7 (1)	2·1 (1)	0·18 (1)	99·7
11	47·6 (3)	0·69 (4)	17·9 (1)	0·06 (2)	7·8 (1)	12·6 (1)	11·0 (1)	2·2 (1)	0·16 (2)	100·3
12	47·7 (3)	0·72 (4)	18·5 (2)	0·02 (1)	8·2 (1)	10·9 (3)	11·3 (2)	2·5 (1)	0·14 (1)	100·2
26	45·6 (3)	0·61 (4)	15·5 (1)	0·02 (1)	8·2 (1)	12·8 (2)	12·6 (2)	1·76 (7)	1·28 (9)	100·3
30A	46·3 (5)	0·58 (5)	17·0 (1)	0·02 (1)	7·5 (3)	11·9 (1)	10·4 (5)	3·1 (3)	1·34 (7)	100·2
30B	45·2 (3)	0·60 (4)	16·5 (2)	0·01 (1)	8·1 (2)	12·0 (2)	10·6 (3)	3·0 (6)	1·52 (3)	99·8
34	46·3 (7)	0·59 (3)	16·2 (4)	0·04 (2)	7·9 (3)	12·9 (2)	11·3 (4)	2·1 (4)	1·0 (2)	99·8
35A	46·5 (3)	0·53 (3)	15·3 (2)	0·07 (1)	7·5 (2)	14·8 (2)	9·6 (2)	1·84 (8)	1·6 (2)	100·1
50	44·1 (5)	0·59 (3)	15·5 (2)	0·03 (1)	8·0 (3)	13·2 (3)	12·5 (1)	1·81 (8)	1·62 (4)	99·8
52A	43·5 (3)	0·58 (1)	14·7 (2)	0·02 (1)	11·4 (2)	13·8 (3)	9·2 (1)	1·91 (5)	1·80 (3)	99·6
56A	46·2 (3)	0·57 (3)	15·2 (1)	0·08 (1)	7·9 (1)	15·6 (1)	9·7 (1)	2·05 (6)	1·15 (8)	100·2
56B	45·8 (2)	0·56 (2)	15·0 (1)	0·09 (2)	7·9 (1)	15·9 (2)	9·6 (1)	2·00 (6)	1·26 (6)	100·0
27	49·0 (7)	0·67 (3)	18·3 (3)	0·06 (2)	4·9 (1)	11·9 (7)	12·1 (2)	2·6 (1)	0·11 (1)	99·8
35B	48·0 (7)	0·61 (3)	18·4 (5)	0·09 (4)	5·1 (6)	12·6 (7)	11·5 (1)	1·78 (9)	0·15 (8)	98·5
52B	47·1 (6)	0·70 (4)	17·7 (2)	0·07 (2)	8·7 (2)	11·9 (4)	10·8 (2)	2·21 (9)	0·16 (1)	99·6
54A	50·1 (2)	0·71 (2)	17·4 (1)	0·11 (1)	5·2 (3)	11·6 (1)	11·9 (2)	2·6 (2)	0·11 (2)	99·9
54B	50·1 (2)	0·73 (4)	18·0 (2)	0·12 (1)	5·3 (2)	11·1 (2)	11·6 (1)	2·52 (7)	0·11 (2)	99·7

*Totals are calculated with S as SO_3.
Numbers in parenthesis are standard deviations (1σ) on the last significant figure.

experiments (roughly in the range $-1 < \Delta FMQ < +2$). However, despite repeated attempts, we could not obtain results at intermediate fO_2 (ideally from quenched glasses saturated and equilibrated simultaneously with both sulfide and sulfate liquids).

DISCUSSION

To the best of our knowledge, the data shown here are the first experimental data for the S content of basaltic melts saturated with a sulfate phase. The most significant result from these experiments is the 10-fold increase in S content between sulfide- and sulfate-saturated basaltic melts at 1300°C and 1 GPa.

Experimental data on the S content of intermediate to felsic melts (ranging from trachyandesites to dacites) saturated in anhydrite were documented by Carroll & Rutherford (1985, 1987) and Luhr (1990). Although their experiments were conducted at lower pressures and temperatures [up to 290 MPa and 1025°C in Carroll & Rutherford (1987); up to 400 MPa and 1000°C in Luhr (1990)] the results showed that the S contents in sulfate-saturated melts were significantly higher than the S content in sulfide-saturated melts. Luhr (1990) extrapolated the increase in the S content at sulfate saturation with rising temperature in his experiments and concluded that 'relatively oxidized (>NNO), vapor-undersaturated basaltic melts at Benioff zone conditions ($T = 1200$°C and $P = 30$ kbar) could contain 1·5 wt % SO_3 and perhaps as much as 2·5 wt % SO_3' (Luhr, 1990, p. 1109). Our results exceed this prediction, showing that at 1300°C and 1 GPa (10 kbar) a basaltic magma can dissolve 1·5 ± 0·2 wt % S (3·75 ± 0·5 wt % SO_3).

Sulfur solubility and the 'sulfur solubility minimum'

A relevant aspect regarding the behavior of S in silicate melts is how the S content changes within the stability fields of sulfide and sulfates. This is relevant because results from experiments equilibrated with gas mixtures show a minimum in the S concentrations in the glasses at about $\Delta FMQ = +1$ (e.g. Fincham & Richardson, 1954; Nagashima & Katsura, 1973; Katsura & Nagashima, 1974). This minimum has been regarded in some cases as a 'sulfur solubility minimum' (e.g. Kress, 1997). Those

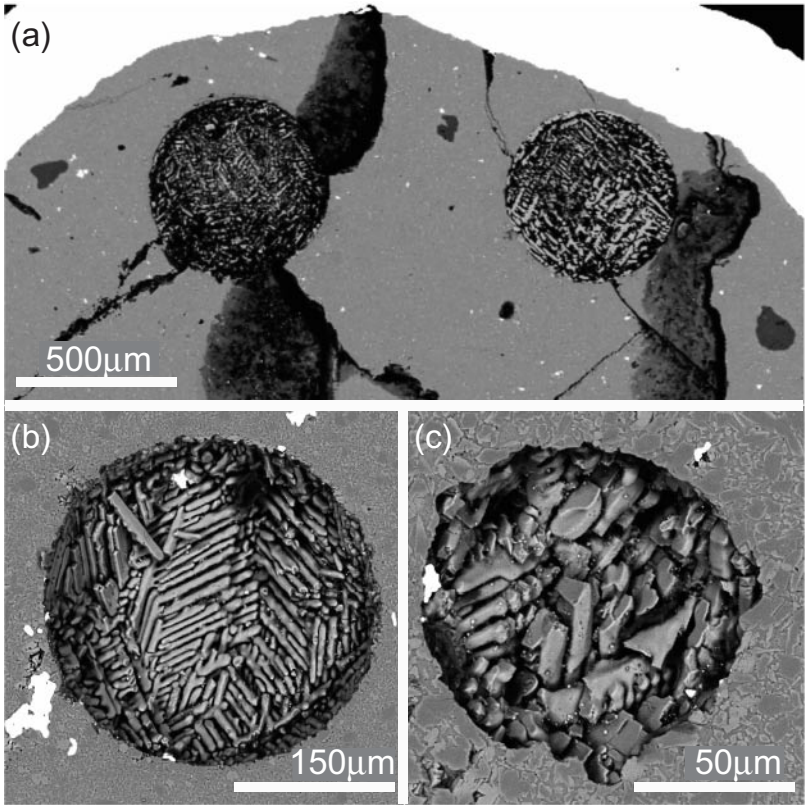

Fig. 1. Backscattered secondary electron images of quenched sulfate blebs. (a) Sections of two large sulfate blebs from run 26, near the edge of the Au–Pd capsule (white, curved band at the top of the picture). (b) Sulfate bleb from run 30A obtained from a mixture of $CaSO_4$ and low-Ca glass as starting material. (c) Sulfate bleb from run 30B obtained from a mixture of $FeSO_4$ and low-Fe glass as starting material. In all cases the round sections of the quenched sulfates are consistent with the presence of these phases as immiscible liquids at run conditions. Qualitative (EDS) analyses of the sulfates showed that they consisted almost entirely of Ca and S and have presumably crystallized as anhydrite upon quenching. Bright white areas in the charge are remnants of the Ir and Pt powders added to the runs.

experiments, however, were not saturated with either sulfide or sulfate (as condensed phases). Therefore, the S concentrations they define do not provide direct information about the S concentrations required to saturate a silicate melt in either sulfides or sulfates (crystalline or liquid). Nonetheless, those results (and the minimum in sulfur content) have applications to the behavior of sulfur in magmas containing a volatile phase after condensed S-bearing phases are eliminated.

In the strict sense, 'solubility' (e.g. for FeS) refers to the maximum amount of a phase (FeS) that a solvent phase (e.g. a silicate melt) can dissolve at a given P and T. The term 'solubility' is phase specific and therefore, for any given P, T and melt composition, the solubility of FeS is different from the solubility of $CaSO_4$, or any other S-bearing phase (as shown in this work). Thus, in a very strict sense, 'sulfur solubility' would apply only to melts saturated with elemental S, which is seldom the case. The term 'solubility' is loosely used to refer to the sulfur content in melts saturated with a S-bearing phase; but because the nature of the saturating phase is critical, the saturating phase needs to be specified clearly and direct extrapolations of the results from one phase to the behavior of other S-bearing phases are not valid.

Experiments equilibrated with gas mixtures have the additional complication that the gases contain several species (e.g. S_2, H_2S, COS, SO_2, SO_3). According to Henry's law, the concentration of these species in the melt is proportional to their fugacities in the gas mixture. Thus, the total sulfur concentration in the melt is the contribution of the S concentrations imposed by each gas species. Carroll & Webster (1994) showed that for fO_2 above $\Delta FMQ = -1$: (1) sulfur is dominantly present as SO_2; (2) the fugacities of reduced species (S_2, H_2S, COS) decrease; (3) fSO_3 increases. Consequently, the variations in the S content for gas-equilibrated experiments reflect mostly: (1) low SO_2 solubility in the melts relative to the other S species; (2) the relative changes in the fugacities of these other S species.

When a silicate melt is simultaneously in equilibrium with a S-bearing condensed phase (e.g. FeS, $CaSO_4$) and a S-bearing gas phase, the total S content in the melt results from their contribution. Thus, as long as sulfides (or sulfates) are present, the S content in the melt will not

Table 5: Compositions of olivines in wt % and oxidation state of the runs

	Sulfate-saturated runs								Sulfate reduction				
Run no.:	26	30B	34	35A	50	52A	56A	56B	27	35B	52B	54A	54B
SiO_2	41·0	41·1	40·7	41·6	40·2	39·9	40·8	40·5	40·7	41·2	39·7	40·4	40·4
Al_2O_3	0·06	0·14	0·12	0·12	n.a.	0·00	0·10	0·13	n.a.	n.a.	0·00	0·03	0·02
Cr_2O_3	n.a.	0·04	0·03	0·04	n.a.	n.a.	n.a.	n.a.	n.a.	0·08	n.a.	n.a.	n.a.
FeO	5·1	6·4	7·4	5·9	6·7	9·0	6·0	5·9	7·1	7·0	9·9	7·4	7·6
MgO	53·1	52·0	51·5	52·3	51·7	50·0	52·7	52·2	50·7	51·5	49·5	51·1	51·1
CaO	0·2	0·1	0·2	0·2	0·2	0·1	0·2	0·2	0·2	0·2	0·1	0·1	0·2
Total	99·4	99·9	100·0	100·2	98·9	99·1	99·7	98·9	98·8	100·0	99·2	99·0	99·2
Si	0·99	0·99	0·99	1·00	0·98	0·98	0·99	0·99	1·00	1·00	0·98	0·99	0·99
Al	0·00	0·00	0·00	0·00	0·00	0·00	0·00	0·00	0·00	0·00	0·00	0·00	0·00
Cr	0·00	0·00	0·00	0·00	0·00	0·00	0·00	0·00	0·00	0·00	0·00	0·00	0·00
Fe^{2+}	0·10	0·13	0·15	0·12	0·14	0·19	0·12	0·12	0·15	0·14	0·20	0·15	0·16
Mg	1·91	1·87	1·86	1·87	1·89	1·84	1·90	1·90	1·85	1·86	1·83	1·87	1·86
Ca	0·00	0·00	0·01	0·00	0·01	0·00	0·00	0·01	0·01	0·01	0·00	0·00	0·00
Total	3·01	3·00	3·01	3·00	3·02	3·02	3·01	3·01	3·00	3·00	3·02	3·01	3·01
Mg no.	0·95	0·94	0·93	0·94	0·93	0·91	0·94	0·94	0·93	0·93	0·90	0·93	0·92
ΔFMQ	3·82	2·59	1·85	2·41	2·22	2·70	2·46	2·50	−1·12	−2·89	−2·87	−1·5	−1·54

*n.a., not analyzed. ΔFMQ is calculated with the analyses in this table and the spinel analyses shown in Table 6.

Table 6: Compositions of spinels

	Sulfate-saturated runs								Sulfate reduction				
Run no.:	26	30B	34	35A	50	52A	56A	56B	27	35B	52B	54A	54B
SiO_2	0·5	0·2	0·7	0·4	0·5	0·4	0·4	0·4	0·5	0·7	0·3	0·8	0·5
TiO_2	0·2	0·1	0·1	0·1	0·2	0·3	0·1	0·1	0·1	0·1	0·2	0·2	0·1
Al_2O_3	48·8	51·5	55·7	45·0	52·9	47·0	45·4	44·7	59·5	53·7	57·1	43·7	44·5
Cr_2O_3	3·3	8·5	5·9	16·2	8·0	6·2	15·2	15·7	9·3	15·3	11·8	25·7	25·4
FeO	23·4	17·7	14·8	16·1	15·5	24·8	16·1	16·3	6·7	6·7	9·5	7·6	6·5
MgO	23·0	22·4	23·5	22·2	22·4	20·3	22·3	22·2	24·3	23·0	21·5	22·2	22·8
Total	99·2	100·5	100·8	100·2	99·5	99·0	99·5	99·5	100·3	99·5	100·3	100·1	99·8
Si	0·014	0·006	0·018	0·012	0·012	0·011	0·012	0·011	0·012	0·019	0·007	0·020	0·012
Ti	0·003	0·002	0·002	0·003	0·003	0·005	0·003	0·003	0·002	0·001	0·003	0·003	0·003
Al	1·505	1·572	1·660	1·409	1·617	1·486	1·425	1·405	1·756	1·636	1·725	1·379	1·399
Cr	0·068	0·174	0·119	0·341	0·164	0·132	0·319	0·331	0·183	0·312	0·239	0·543	0·536
Fe^{3+}*	0·392	0·237	0·179	0·221	0·188	0·351	0·227	0·235	0·033	0·011	0·014	0·031	0·035
Fe^{2+}	0·120	0·146	0·133	0·136	0·149	0·205	0·130	0·129	0·107	0·133	0·190	0·139	0·110
Mg	0·897	0·863	0·888	0·878	0·866	0·811	0·884	0·885	0·907	0·887	0·821	0·885	0·905
$Fe^{3+}/\Sigma Fe$	0·77	0·62	0·57	0·62	0·56	0·63	0·64	0·65	0·24	0·08	0·07	0·18	0·24

*Fe^{3+} estimated from stoichiometry.

Table 7: Compositions of clinopyroxenes

Run no.:	2	3	4	5	7	12	26	34	27
SiO_2	50·1	51·7	48·6	50·6	49·5	50·3	48·3	47·6	48·3
TiO_2	0·262	0·194	0·509	0·225	0·371	0·240	0·221	0·694	0·636
Al_2O_3	10·3	9·7	14·2	10·4	11·6	10·3	9·1	16·7	17·8
Cr_2O_3	0·151	0·240	0·097	0·282	0·099	0·214	0·133	0·043	0·063
FeO	5·6	5·1	6·2	4·5	5·7	4·8	6·6	8·0	4·7
MgO	19·1	21·8	16·9	19·8	17·8	19·3	18·3	14·0	12·7
CaO	13·8	12·8	13·1	14·5	14·4	14·5	16·5	13·0	14·1
Na_2O	0·574	0·532	0·706	0·547	0·694	0·539	0·483	1·512	1·491
Total	99·9	102·0	100·3	100·8	100·1	100·1	99·6	101·5	99·9
Si	1·795	1·802	1·733	1·791	1·773	1·794	1·766	1·693	1·720
Ti	0·007	0·005	0·014	0·006	0·010	0·006	0·006	0·019	0·017
Al	0·436	0·398	0·596	0·432	0·488	0·432	0·392	0·700	0·748
Cr	0·004	0·007	0·003	0·008	0·003	0·006	0·004	0·001	0·002
Fe	0·168	0·149	0·186	0·135	0·170	0·142	0·203	0·237	0·140
Mg	1·020	1·133	0·898	1·043	0·952	1·025	0·996	0·742	0·672
Ca	0·528	0·478	0·500	0·550	0·553	0·556	0·645	0·495	0·537
Na	0·040	0·036	0·049	0·038	0·048	0·037	0·034	0·104	0·103
Total	3·998	4·008	3·978	4·002	3·996	3·999	4·047	3·991	3·940

Table 8: Compositions of orthopyroxenes

	Sulfide-saturated runs							Sulfate-saturated runs					Sulfate reduction	
Run no.:	2	3	4	5	7	11	12	26	30A	30B	34	35A	27	35B
SiO_2	52·3	52·4	51·7	52·1	51·9	52·2	52·8	51·5	52·2	52·6	51·6	52·6	52·8	54·0
TiO_2	0·132	0·153	0·126	0·105	0·109	0·116	0·099	0·086	0·095	0·074	0·110	0·106	0·099	0·109
Al_2O_3	8·8	9·8	9·8	8·9	9·8	9·7	9·0	8·3	8·8	8·2	9·0	8·1	8·0	8·3
Cr_2O_3	0·213	0·441	0·258	0·339	0·281	0·475	0·309	0·076	0·410	0·536	0·317	0·566	0·395	0·467
FeO	7·1	6·1	6·9	6·2	6·7	5·8	6·1	6·4	6·3	6·2	6·3	5·5	4·8	5·0
MgO	29·2	30·2	29·2	29·8	29·4	29·9	30·3	32·1	31·9	32·1	31·5	32·3	32·0	32·3
CaO	2·4	2·5	2·3	2·5	2·2	2·2	2·4	2·2	1·2	0·9	1·7	1·2	1·9	1·6
Na_2O	0·115	0·118	0·117	0·096	0·097	0·087	0·089	0·069	0·055	0·054	0·079	0·045	0·059	0·064
Total	100·2	101·7	100·4	100·1	100·5	100·5	101·2	100·7	100·9	100·6	100·8	100·5	100·1	101·9
Si	1·816	1·788	1·791	1·807	1·796	1·799	1·810	1·781	1·792	1·810	1·781	1·808	1·818	1·825
Ti	0·003	0·004	0·003	0·003	0·003	0·003	0·003	0·002	0·002	0·002	0·003	0·003	0·003	0·003
Al	0·359	0·396	0·401	0·366	0·398	0·392	0·364	0·338	0·357	0·331	0·368	0·329	0·324	0·330
Cr	0·006	0·012	0·007	0·009	0·008	0·013	0·008	0·002	0·011	0·015	0·009	0·015	0·011	0·012
Fe	0·208	0·174	0·200	0·179	0·193	0·168	0·176	0·185	0·180	0·177	0·182	0·159	0·138	0·142
Mg	1·512	1·536	1·511	1·542	1·515	1·535	1·549	1·654	1·633	1·646	1·619	1·656	1·645	1·629
Ca	0·089	0·091	0·085	0·094	0·082	0·082	0·089	0·082	0·043	0·034	0·065	0·046	0·072	0·058
Na	0·008	0·008	0·008	0·006	0·007	0·006	0·006	0·005	0·004	0·004	0·005	0·003	0·004	0·004
Total	4·002	4·008	4·006	4·006	4·002	3·998	4·004	4·049	4·023	4·018	4·031	4·018	4·014	4·003

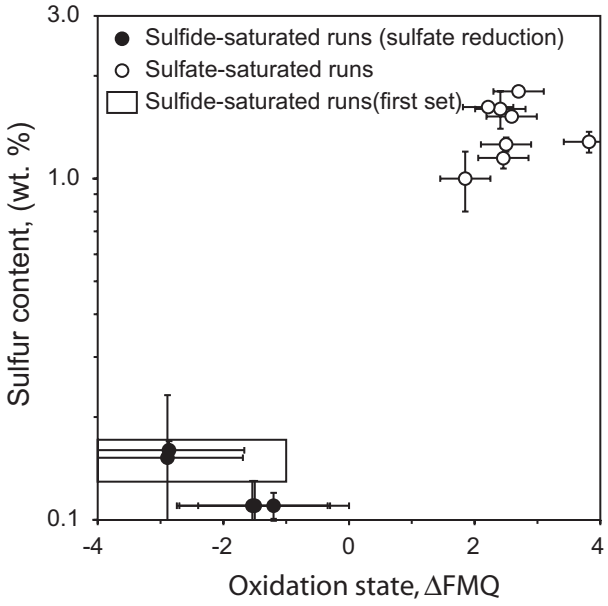

Fig. 2. S concentration in run-product glasses plotted as a function of oxidation state, from sulfide- and sulfate-saturated assemblages. S concentrations measured by EMPA. Oxidation states, relative to the FMQ buffer, were calculated from olivine and spinel compositions using the oxybarometer calibration of Ballhaus *et al.* (1990, 1991). Error bars are 1σ standard deviation for S concentrations and the uncertainties associated with the oxybarometer calibration used (±0·4 above FMQ and approximately ±1·2 near ΔFMQ = −3; Ballhaus *et al.*, 1991). The width of the rectangular box in the lower left corner indicates the range in S concentration for the first set of experiments. For those experiments, the oxidation state was not estimated but the presence of graphite indicates that they equilibrated at fO_2 below ΔFMQ = −1.

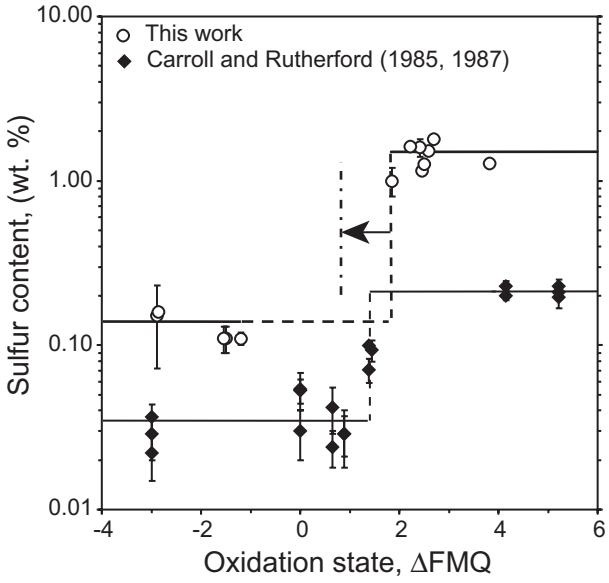

Fig. 3. Comparison of the S concentration as a function of fO_2 in basaltic melts (at 1300°C and 1 GPa; this work) and in trachyandesites (at 200 MPa and for $927 < T < 1027$°C; Carroll & Rutherford, 1985, 1987). The data from Carroll & Rutherford (1985, 1987) include only glasses with FeO < 17 wt % to show only the effect of changes in fO_2. The arrow indicates the expected shift in the stability of sulfate phases with decreasing silica activity, based on data from Sisson (2003).

show the changes shown in gas-equilibrated experiments and no 'sulfur solubility minimum' would exist. This can be seen in Fig. 3, which compares the sulfur content at sulfide and sulfate saturation of trachyandesitic melts (Carroll & Rutherford, 1985, 1987) and basaltic melts (this work). The data for sulfide-saturated experiments from Carroll & Rutherford (1985, 1987) clearly show that S concentration in trachyandesitic melts at sulfide saturation remain constant at about 0·350 wt %, independent of changes in fO_2. This was also demonstrated by O'Neill & Mavrogenes (2002), who showed that the sulfur concentration at sulfide saturation was independent of fO_2.

Transition from sulfide to sulfate stability

The relevance to magmatic processes of the increase in the S content in basaltic melts from sulfide saturation to sulfate saturation depends on the fO_2 at which sulfides oxidize to sulfates. For any given composition, this would be constrained by the lowest fO_2 at which sulfates are stable and the highest fO_2 at which sulfides are stable. The results of our experiments show that sulfates were stable at fO_2 as low as ΔFMQ = +1·85, but the highest fO_2 at which sulfides are stable is probably higher than that shown by our data (ΔFMQ = −1·12), which is rather an indication of the fO_2 imposed by the presence of graphite.

Extrapolation of the sulfide–sulfate boundary from other experimental work was not attempted because the effect of composition is significant. Stormer & Carmichael (1971) showed that silica undersaturation favors sulfide oxidation at a given fO_2 because in reactions such as

$$\underset{\text{pyrrhotite}}{FeS} + \underset{\text{aegirine}}{2NaFeSi_2O_6} + \underset{\text{albite}}{6NaAlSi_3O_8} + 2O_2 = \underset{\text{nosean}}{Na_8Al_6Si_6O_{24}(SO_4)} + \underset{\text{magnetite}}{Fe_3O_4} + \underset{\text{liquid}}{16SiO_2} \quad (1)$$

a decrease in the activity of silica (at a fixed fO_2) would force the reaction to the right, favoring the formation of nosean.

An analogous reaction, more appropriate for mantle assemblages, can be written as

$$FeS^{sulfide} + Fe_2SiO_4^{olivine} + 5/2O_2 = SO_3^{melt} + Fe_3O_4^{spinel} + SiO_2^{melt}. \quad (2)$$

As in equation (1), a decrease in the activity of silica at a fixed fO_2 promotes S dissolution in the silicate melt as SO_3 (which eventually could result in the precipitation of

sulfate-bearing phases) at the expense of the troilite component in the sulfides.

Carroll & Rutherford (1987) used a similar reaction,

$$3FeS + 3CaSiO_3 + 13/2O_2 = 3CaSO_4 + Fe_3O_4 + 3SiO_2 \quad (3)$$

to analyze qualitatively the compositional effects on sulfide–sulfate equilibria. They calculated an fO_2 of $\Delta NNO = +1$ ($\Delta FMQ = +1{\cdot}7$) for reaction (3) by fixing the activities of all condensed phases to unity. Using this equilibrium they concluded that a decrease in silica activity would make sulfates stable at lower fO_2 whereas a decrease in the activity of wollastonite would have the opposite effect.

In more complex systems, the activities of components in condensed phases will be different from unity and, therefore, fO_2 for the transition from sulfide to sulfate will differ from those defined by reaction (1), (2) or (3) using pure components. Systematic experimental studies are needed to properly constrain the transition from sulfide to sulfate as a function of fO_2, P, T, and melt composition. Estimates of the effect of composition can be made, for example, using experimental data from Carroll & Rutherford (1987) and Scaillet *et al.* (1998), in which trachyandesites and dacites (respectively) were used as starting materials. Experiments 142a and 141a of Carroll & Rutherford (1987) showed that, at 204 MPa and 927°C, anhydrite was stable at fO_2 as low as $\Delta FMQ = +1{\cdot}39$ and pyrrhotite was stable at fO_2 as high as $\Delta FMQ = +0{\cdot}89$ (Fig. 3). Experiment 42b of Scaillet *et al.* (1998) showed that anhydrite was present at fO_2 as low as $\Delta FMQ = +1{\cdot}9$ under similar P–T conditions (225 MPa and 899°C). Thus, it appears that the change in composition from dacite to trachyandesite lowers the fO_2 needed to stabilize anhydrite by about 0·5 log fO_2 units.

We speculate that for basaltic melts the change from sulfide to sulfate stability occurs at fO_2 of about $\Delta FMQ = +1{\cdot}8$ (based on our results) and that decrease in silica activity could push this to fO_2 as low as $\Delta FMQ = +1$ as shown by Sisson (2003) for basanites from Hawaii (Fig. 3).

Implications for magmatic processes

The marked increase in the S content with increasing oxidation state has significant implications for the behavior of S during partial melting of the mantle and during magmatic evolution. Because highly siderophile elements (Rh, Ru, Pd, Re, Os, Ir, Pt, and Au) are dominantly hosted in sulfide phases (Mitchell & Keays, 1981), generation of silicate melts enriched in precious metals is favored by elimination of sulfides. Sulfide dissolution, either by large degrees of melting (e.g. Keays, 1995) or by two stages of melting (e.g. Wyborn & Sun, 1994), is the most commonly proposed mechanism for sulfide elimination.

The importance of oxidation as an alternative mechanism for sulfide elimination in primitive magmas has been discussed qualitatively (e.g. Richards *et al.*, 1991; Sillitoe, 1997; Mungall, 2002). Sulfide elimination by oxidation of the mantle source is consistent with hypotheses that link Au-rich and high Au/Cu magmatic–hydrothermal ore deposits with oxidized magmas (e.g. Richards, 1995; Sillitoe, 1997). Parkinson & Arculus (1999) estimated that the fO_2 of arc magmas at their source ranged from $\Delta FMQ = +0{\cdot}5$ to $\Delta FMQ = +1{\cdot}7$, and Blatter & Carmichael (1998) showed that fO_2 in the subarc upper mantle can reach $\Delta FMQ = +2{\cdot}4$. Thus, it can be inferred that in the most oxidized arc sources sulfide phases would not be stable. Under such conditions chalcophile and siderophile element behavior will be controlled by alloy–melt or oxide–melt equilibria, and some elements would probably be incompatible. Evidence from lherzolites and harzburgites from orogenic massifs indicates that 'except for Pd and Au, the PGE reside in mantle sulfides as melting-resistant atomic clusters or micro alloys' (Lorand *et al.*, 1999, p. 957). Capobianco *et al.* (1994) showed that, in the absence of sulfides, Pd behaves as an incompatible element whereas Ru and Rh are compatible in oxide phases. Thus, magma generation in oxidized sources in which sulfides are not stable would fractionate Au and Pd from other siderophile elements. A low activity of silica in the melt (e.g. produced by low degrees of partial melting and relatively high alkali contents) would allow for sulfide elimination at lower oxidation states, which is consistent with the association of Au-rich deposits with oxidized alkalic magmas (e.g. Richards, 1995). An example of this was shown by Sisson (2003), who found a native gold grain in basanites from Hawaii. The fO_2 estimated in these basanites is $\Delta FMQ = +0{\cdot}9$, but this was sufficient to resorb magmatic sulfides and liberate gold hosted in them. In fact, Sisson (2003) found that the proportion of sulfate in the basanites increased with decreasing silica, rather than with increasing fO_2.

Even if magmas are generated within the stability field of sulfides, many magmas become oxidized enough during ascent and evolution to preclude, or reverse, sulfide saturation. For example, Metrich *et al.* (1999) and de Hoog *et al.* (2001) documented S concentrations in basaltic glasses from subduction zones approaching 3000 ppm, and Wallace (2002) measured up to 6000 ppm S in olivine-hosted melt inclusions from cinder cones associated with Popocatepetl (Mexico). These S contents greatly exceed the S concentration predicted in sulfide-saturated basaltic melts but are within the range of S concentrations expected for oxidized systems as shown in this work. Ballhaus (1993) showed that the fO_2 of island-arc magmas ranged from $\Delta FMQ = +1$ to $FMQ = +3$ and that back-arc basalts and island-arc basalts can reach $\Delta FMQ = +2$. Thus, at oxidation states

above those at which sulfide phases are stable, S in the form of dissolved sulfate will behave as an incompatible element and its concentration in the melt will increase with crystallization and fractionation until: (1) sufficiently high concentrations are reached to precipitate anhydrite; (2) another sulfate-bearing phase (e.g. nosean, haüyne, apatite) saturates; or (3) a vapor phase (S-rich) exsolves.

The significant increase in S content of the melt between sulfide and sulfate saturation may also help explain high-S degassing in some volcanoes. Estimates (de Hoog *et al.*, 2003) of the fO_2 of basalts associated with the Pinatubo eruption (based on Cr-spinel-bearing olivine) yield $\Delta NNO = +1{\cdot}4$ (roughly $\Delta FMQ = +2{\cdot}1$) and are almost identical to those of the dacitic magma erupted (roughly $\Delta FMQ = +2{\cdot}3$). These estimates indicate that the basaltic melt and the dacitic magma had similar high oxidation states. At such high oxidation states, no sulfide phases would be present and all available S should be dissolved in the melt (dominantly as sulfate species) or present as a sulfate phase (e.g. anhydrite). Because the S content at sulfate saturation decreases sharply with falling temperature and decreasing pressure (Carroll & Rutherford, 1987; Luhr, 1990) decompression and cooling of oxidized, S-rich basaltic melts as they ascend and mix with overlying hydrous dacitic magma to produce a hybrid andesite (Pallister *et al.*, 1996) should result in saturation of anhydrite. However, sulfate partitions preferentially into a hydrous phase and water exsolution would strip the melt of most of its S (as SO_2; Keppler, 1999). Because of the large amounts of S that can be dissolved in oxidized basaltic melts, relatively small amounts of basalt could provide large quantities of S to exsolved volatile phases.

CONCLUSIONS

The results of this work show that changes in fO_2 have a significant impact on the behavior of S in basaltic systems, producing a 10-fold increase in the S content of basaltic magmas at high fO_2. Thus, modeling of physico-chemical processes in which S-bearing phases are important (e.g. sulfide saturation and elimination, melt enrichment in precious metals, S-rich explosive volcanism) needs to consider both the range in fO_2 in which sulfide oxidizes to sulfate and the increase in the S content related to this change.

ACKNOWLEDGEMENTS

This research was supported by NSERC grants to R.W.L. and J.P.R. Additional financial support in the form of a Geological Society of America Student Research Grant, C. M. Scarfe Scholarships in Experimental Petrology from the University of Alberta, and a Canadian Association of Petroleum Producers Scholarship to P.J.J. are gratefully acknowledged. We thank R. J. Arculus and an anonymous reviewer for their comments, which helped improve this work. We also thank M. Wilson for the editorial management.

REFERENCES

Ballhaus, C. (1993). Redox states of lithospheric and asthenospheric upper mantle. *Contributions to Mineralogy and Petrology* **114**, 331–348.

Ballhaus, C., Berry, R. F. & Green, D. H. (1990). Oxygen fugacity controls in the Earth's upper mantle. *Nature* **348**, 437–440.

Ballhaus, C., Berry, R. F. & Green, D. H. (1991). High-pressure experimental calibration of the olivine–orthopyroxene–spinel oxygen geobarometer: implications for the oxidation state of the upper mantle. *Contributions to Mineralogy and Petrology* **107**, 27–40.

Blatter, D. L. & Carmichael, I. S. E. (1998). Hornblende peridotite xenoliths from central Mexico reveal the highly oxidized nature of subarc upper mantle. *Geology* **26**, 1035–1038.

Boyd, F. R. & England, J. L. (1960). Apparatus for phase-equilibrium measurements at pressures up to 50 kilobars and temperatures up to 1750°C. *Journal of Geophysical Research* **65**, 741–748.

Brauns, R. (1914). Skapolithführende Auswürflinge aus dem Laacher Seegebiet. *Neues Jahrbuch für Mineralogie, Geologie und Paläeontologie* **39**, 79–125.

Canil, D., Virgo, D. & Scarfe, C. M. (1990). Oxidation state of mantle xenoliths from British Columbia, Canada. *Contributions to Mineralogy and Petrology* **104**, 453–462.

Capobianco, C. J., Hervig, R. L. & Drake, M. J. (1994). Experiments on crystal/liquid partitioning of Ru, Rh and Pd for magnetite and hematite solid solutions crystallized from silicate melt. *Chemical Geology* **113**, 23–43.

Carroll, M. R. & Rutherford, M. J. (1985). Sulfide and sulfate saturation in hydrous silicate melts. *Journal of Geophysical Research* **90**, C601–C612.

Carroll, M. R. & Rutherford, M. J. (1987). The stability of igneous anhydrite: experimental results and implications for S behavior in the 1982 El Chichón trachyandesite and other evolved magmas. *Journal of Petrology* **28**, 781–801.

Carroll, M. R. & Rutherford, M. J. (1988). Sulfur speciation in hydrous experimental glasses of varying oxidation state: results from measured wavelength shifts of sulfur X-rays. *American Mineralogist* **73**, 845–849.

Carroll, M. R. & Webster, J. D. (1994). Solubilities of sulfur, noble gases, nitrogen, chlorine, and fluorine in magmas. In: Carroll, M. R. & Holloway, J. R. (eds) *Volatiles in Magmas. Mineralogical Society of America, Reviews in Mineralogy* **30**, 231–279.

De Hoog, J. C. M., Mason, P. R. D. & van Bergen, M. J. (2001). S and chalcophile elements in subduction zones: constraints from a laser ablation ICP-MS study of melt inclusions from Galunggung Volcano, Indonesia. *Geochimica et Cosmochimica Acta* **65**, 3147–3164.

De Hoog, J. C. M., Hattori, K. H. & Hoblitt, R. P. (2003). Oxidized, S-rich mafic magma at Mount Pinatubo, Philippines. (EGS–AGU 2003 Spring meeting abstracts.) *Geophysical Research Abstracts* **5**, 01660.

De Silva, S. L. & Zielinski, XX. (1998). Global influence of the AD1600 eruption of Huaynaputina, Peru. *Nature* **393**, 455–458.

Dunn, T. (1993). The piston-cylinder apparatus. *Mineralogical Association of Canada, Short Course Handbook* **21**, 39–94.

Fincham, C. J. B. & Richardson, F. D. (1954). The behaviour of sulphur in silicate and aluminate melts. *Proceeding of the Royal Society of London, Series A* **223**, 40–61.

Fujii, T. & Scarfe, C. M. (1982). Petrology of ultramafic nodules from West Kettle River, near Kelowna, southern British Columbia. *Contributions to Mineralogy and Petrology* **80**, 297–306.

Gaetani, G. A. & Grove, T. L. (1998). The influence of water on melting of mantle peridotite. *Contributions to Mineralogy and Petrology* **131**, 323–346.

Gerlach, T. M., Westrich, H. R. & Symonds, R. B. (1996). Preeruption vapor in magma of the climactic Mount Pinatubo eruption; source of giant stratospheric S dioxide cloud. In: Newhall, C. G. & Punongbayan, R. S. (eds) *Fire and Mud: Eruptions and Lahars of Mount Pinatubo, Philippines*. Quezon City: Philippine Institute of Volcanology and Seismology; Seattle: University of Washington Press, pp. 415–433.

Gurenko, A. A. & Schmincke, H.-U. (1998). Petrology, geochemistry, S, Cl, and F abundances, and S oxidation state of sideromelane glass shards from Pleistocene ash layers north and south of Gran Canaria (ODP Leg 157). *Contributions to Mineralogy and Petrology* **131**, 95–110.

Gurenko, A. A. & Schmincke, H.-U. (2000). S concentrations and its speciation in Miocene basaltic magmas north and south of Gran Canaria (Canary Islands): constraints from glass inclusions in olivine and clinopyroxene. *Geochimica et Cosmochimica Acta* **64**, 2321–2337.

Hattori, K. H. (1993). High-S magma, a product of fluid discharge from underlying mafic magma: evidence from Mount Pinatubo, Philippines. *Geology* **21**, 1083–1086.

Haughton, D. R., Roeder, P. L. & Skinner, B. J. (1974). Solubility of S in mafic magmas. *Economic Geology* **69**, 451–466.

Holloway, J. R., Pan, V. & Gudmundsson, G. (1992). High-pressure fluid-absent melting experiments in the presence of graphite: oxygen fugacity, ferric/ferrous ratio and dissolved CO_2. *European Journal of Mineralogy* **4**, 105–114.

Holzheid, A. & Grove, T. L. (2002). Sulfur saturation limits in silicate melts and their implications for core formation scenarios for terrestrial planets. *American Mineralogist* **87**, 227–237.

Jaques, A. L. & Green, D. H. (1980). Anhydrous melting of peridotite at 0–15 kbar pressure and the genesis of tholeiitic basalts. *Contributions to Mineralogy and Petrology* **73**, 287–310.

Jarosevich, E., Nelen, J. A. & Norberg, J. A. (1980). Reference samples for electron microprobe analysis. *Geostandards Newsletter* **4**, 43–47.

Katsura, T. & Nagashima, S. (1974). Solubility of S in some magmas at 1 atmosphere. *Geochimica et Cosmochimica Acta* **38**, 517–531.

Keays, R. R. (1995). The role of komatiitic and picritic magmatism and S-saturation in the formation of ore deposits. *Lithos* **34**, 1–18.

Keppler, H. (1999). Experimental evidence for the source of excess S in explosive volcanic eruptions. *Science* **284**, 1652–1654.

Kilinc, A. Carmichael, I. S. E., Rivers, M. L. & Sack, R. O. (1983). The ferric–ferrous ration of natural silicate liquids equilibrated in air. *Contributions to Mineralogy and Petrology* **83**, 136–140.

Kress, V. C. (1997). Magma mixing as a source for Pinatubo sulphur. *Nature* **389**, 591–593.

Kushiro, I. (1976). Changes in viscosity and structure of melt of $NaAlSi_2O_6$ composition at high pressures. *Journal of Geophysical Research* **81**, 6347–6350.

Lindgren, W. & Ransome, F. L. (1906). Geology and gold deposits of the Cripple Creek district, Colorado. *US Geological Survey Professional Paper* **54**.

Lorand, J.-P., Pattou, L. & Gros, M. (1999). Fractionation of platinum-group elements and gold in the upper mantle: a detailed study in Pyrenean orogenic lherzolites. *Journal of Petrology* **40**, 957–981.

Luhr, J. F. (1990). Experimental phase relations of water- and S-saturated arc magmas and the 1982 eruption of El Chichón volcano. *Journal of Petrology* **31**, 1071–1114.

Luhr, J. F. & Varekamp, J. C. (1984). El Chichon volcano, Chiapas, Mexico (Introduction to the special volume). *Journal of Volcanology and Geothermal Research* **23**, vii.

Luhr, J. F., Carmichael, I. S. E. & Varekamp, J. C. (1984). The 1982 eruptions of El Chichón volcano, Chiapas, Mexico: mineralogy and petrology of the anhydrite-bearing pumice. *Journal of Volcanology and Geothermal Research* **23**, 69–108.

Massalski, T. B. (ed.) (1986). *Binary Alloy Phase Diagrams*. Metals Park, OH: American Society for Metals.

Matthews, S. J., Moncrieff, D. H. D. & Carroll, M. R. (1999). Empirical calibration of the sulphur valence oxygen barometer from natural and experimental glasses: method and applications. *Mineralogical Magazine* **63**, 421–431.

Mattioli, G. S. & Wood, B. J. (1988). Magnetite activities across the $MgAl_2O_4$–Fe_3O_4 spinel join, with application to thermobarometric estimates of upper mantle oxygen fugacity. *Contributions to Mineralogy and Petrology* **98**, 148–162.

Mavrogenes, J. A. & O'Neill, H. St. C. (1999). The relative effects of pressure, temperature and oxygen fugacity on the solubility of sulfide in mafic magmas. *Geochimica et Cosmochimica Acta* **63**, 1173–1180.

McDonough, W. F. & Sun, S.-s. (1995). The composition of the Earth. *Chemical Geology* **120**, 223–253.

Metrich, N. & Clocchiatti, R. (1996). S abundance and its speciation in oxidized alkaline melts. *Geochimica et Cosmochimica Acta* **60**, 4151–4160.

Metrich, N., Schiano, P., Clocchiatti, R. & Maury, R. C. (1999). Transfer of S in subduction settings: an example from Batan Island (Luzon volcanic arc, Philippines). *Earth and Planetary Science Letters* **167**, 1–14.

Mitchell, R. H. & Keays, R. R. (1981). Abundance and distribution of gold, palladium and iridium in some spinel and garnet lherzolites: implications for the nature and origin of precious metal-rich intergranular components in the upper mantle. *Geochimica et Cosmochimica Acta* **45**, 2425–2442.

Mungall, J. E. (2002). Roasting the mantle: slab melting and the genesis of major Au and Au-rich Cu deposits. *Geology* **30**, 915–918.

Nagashima, S. & Katsura, T. (1973). The solubility of S in Na_2O–SiO_2 melts under various oxygen partial pressures at 1100°C, 1250°C, and 1300°C. *Bulletin of the Chemical Society of Japan* **46**, 3099–3103.

Newhall, C. G., Daag, A. S., Delfin, F. G., Hoblitt, R. P., McGeehin, J., Pallister, J. S., Regalado, M. T., Rubin M., Tubianosa, B. S., Tamayo, R. A. & Umbal, J. V. (1996). Eruptive history of Mount Pinatubo. In: Newhall, C. G. & Punongbayan, R. S. (eds) *Fire and Mud: Eruptions and Lahars of Mount Pinatubo, Philippines*. Quezon City: Philippine Institute of Volcanology and Seismology; Seattle: University of Washington Press, pp. 165–195.

Nilsson, K. & Peach, C. L. (1993). S speciation, oxidation state, and S concentration in back-arc magmas. *Geochimica et Cosmochimica Acta* **57**, 3807–3813.

O'Neill, H. St. C. & Mavrogenes, J. A. (2002). The sulfide capacity and the S content at sulfide saturation of silicate melts at 1400°C and 1 bar. *Journal of Petrology* **43**, 1049–1087.

O'Neill, H. St. C. & Wall, V. J. (1987). The olivine–orthopyroxene–spinel oxygen barometer, the nickel precipitation curve, and the oxygen fugacity of the Earth's upper mantle. *Journal of Petrology* **28**, 1169–1191.

Pallister, J. S., Hoblitt, R. P., Meeker, G. P., Knight, R. J. & Siems, D. F. (1996) Magma mixing at Mount Pinatubo: petrographic and chemical evidence from the 1991 deposits. In: Newhall, C. G. & Punongbayan, R. S. (eds) *Fire and Mud: Eruptions and Lahars of Mount Pinatubo, Philippines*. Quezon City: Philippine Institute of Volcanology and Seismology; Seattle: University of Washington Press, pp. 687–731.

Palmer, A. S., van Ommen, T. D., Curran, M. A. J., Morgan, V., Souney, J. M. & Mayewski, P. A. (2001). High-precision dating of volcanic events (A.D. 1301–1995) using cores from Law Dome, Antarctica. *Journal of Geophysical Research, D, Atmospheres* **106**, 28089–28095.

Parkinson, I. J. & Arculus, R. J. (1999). The redox state of subduction zones: insights from arc-peridotites. *Chemical Geology* **160**, 409–423.

Poulson, S. R. & Ohmoto, H. (1990). An evaluation of the solubility of sulfide S in silicate melts from experimental data and natural samples. *Chemical Geology* **85**, 57–75.

Richards, J. P. (1995). Alkalic-type epithermal gold deposits—a review. In: *Magmas, Fluids, and Ore Deposits, Mineralogical Association of Canada Short Course* **23**, 367–400.

Richards, J. P., McCulloch, M. T., Chappell, B. W. & Kerrich, R. (1991). Sources of metals in the Porgera gold deposit, Papua New Guinea: evidence from alteration, isotope, and noble metal geochemistry. *Geochimica et Cosmochimica Acta* **55**, 565–580.

Robinson, J. A. C., Wood, B. J. & Blundy, J. D. (1998). The beginning of melting of fertile and depleted peridotite at 1·5 GPa. *Earth and Planetary Science Letters* **155**, 97–111.

Roeder, P. L. & Emslie, R. F. (1970). Olivine–liquid equilibrium. *Contributions to Mineralogy and Petrology* **29**, 275–289.

Scaillet, B., Clemente, B., Evans, B. W. & Pichavant, M. (1998). Redox control of sulfur degassing in silicic magmas. *Journal of Geophysical Research* **103**, 23937–23949.

Self, S., Zhao, J., Holasek, R. E., Torres, R. C. & King, A. J. (1996). The atmospheric impact of the 1991 Mount Pinatubo eruption. In: Newhall, C. G. & Punongbayan, R. S. (eds) *Fire and Mud: Eruptions and Lahars of Mount Pinatubo, Philippines*. Quezon City: Philippine Institute of Volcanology and Seismology; Seattle: University of Washington Press, pp. 1098–1115.

Sillitoe, R. H. (1997). Characteristics and controls of the largest porphyry copper–gold and epithermal gold deposits in the circum-Pacific region. *Australian Journal of Earth Sciences* **44**, 373–388.

Sisson, T. W. (2003). Native gold in a Hawaiian alkalic magma. *Economic Geology* **95**, 643–648.

Stormer, J. C. & Carmichael, I. S. E. (1971). The free energy of sodalite and the behavior of chloride, fluoride and sulfate in silicate magmas. *American Mineralogist* **56**, 292–306.

Stothers, R. B. (1984). The great Tambora eruption in 1815 and its aftermath. *Science* **224**, 1191–1198.

Ulmer, P. (1989). The dependence of the Fe^{2+}–Mg cation-partitioning between olivine and basaltic liquid on pressure, temperature and composition: an experimental study to 30 kbars. *Contributions to Mineralogy and Petrology* **101**, 261–273.

Ulmer, P. & Luth, R. W. (1991). The graphite–COH fluid equilibrium in P, T, fO_2 space: an experimental determination to 30 kbar and 1600°C. *Contributions to Mineralogy and Petrology* **106**, 265–272.

Wallace, P. J. (2002). Volatile constituents and vapor saturation: integrating petrological and remote sensing perspectives to understand magmatic volatile budgets. *EOS Transactions, American Geophysical Union* **83**(47), abstract V52D-13.

Windom, K. E. & Boettcher, A. L. (1976). The effect of reduced activity of anorthite on the reaction grossular + quartz = anorthite + wollastonite; a model for plagioclase in the Earth's lower crust and upper mantle. *American Mineralogist* **61**, 889–896.

Wood, B. J. & Virgo, D. (1989). Upper mantle oxidation state: ferric iron contents of lherzolite spinels by ^{57}Fe Mössbauer spectroscopy and resultant oxygen fugacities. *Geochimica et Cosmochimica Acta* **53**, 1277–1291.

Wyborn, D. & Sun, S.-S. (1994). Sulphur-undersaturated magmatism—a key factor for generating magma-related copper–gold deposits: *AGSO Research Newsletter* (November), 7–8.

View publication stats